Cold Regions Science and Technology 167 (2019) 102856

Contents lists available at ScienceDirect

Cold Regions Science and Technology

journal homepage: www.elsevier.com/locate/coldregions

A multivariate freezing-thawing depth prediction model for spring load restriction

Ting Bao[a], Zhen Liu (Leo)[c,*], John Bland[b]

[a] Department of Civil and Environmental Engineering, Michigan Technological University, 1400 Townsend Drive, Dow 854, Houghton, MI 49931, United States of America
[b] Computer Science, Michigan Technological University, 1400 Townsend Drive, Houghton, MI 49931, United States of America
[c] Department of Civil and Environmental Engineering, Michigan Technological University, 1400 Townsend Drive, Dillman 201F, Houghton, MI 49931, United States of America

ARTICLE INFO

Keywords:
Freezing/thawing depth
Spring load restriction
Freezing/thawing index
Field data
Freezing/thawing depth prediction

ABSTRACT

Road damages induced by heavily loaded truck traffic during the spring thaw are a major road distress in cold regions. To minimize these damages, Spring Load Restriction (SLR) is widely applied in the U.S., Canada, and other countries during the early thawing season by controlling the movement of freight-carrying trucks and heavy equipment travel until the thawing ends. Most SLR policies rely on the Freezing Depth (FD) and Thawing Depth (TD), especially the latter one. Therefore, accurate predictions of FD and TD are important to prevent both the extensive damage to the pavement due to the late placement or early removal of SLR and the economic loss of road users due to an unnecessarily long SLR period. Here, we propose a new multivariate model for predicting FD and TD in support of SLR decision-making. The model gives a curving surface of FD and TD in a 3-dimensional space, instead of 2-dimensional in traditional methods, by considering both the freezing and thawing indices in the entire freeze-thaw cycle. For model evaluations, yearly field data measured at five typical sites from 104 sites in Michigan were adopted. The evaluation results showed that the proposed model is accurate in predicting FD and TD for most sites. Compared to the previous TD predictions in the existing study, the TD predictions with the proposed model have been significantly improved. In addition, this study provides field data that have not been reported earlier in the literature and that can be used for validating other prediction models. The reported work is ready for practice for roadways in cold regions to support SLR decision-making.

1. Introduction

Spring Load Restriction (SLR) policies that limit the axle loads of trucks have been implemented in many states of the U.S. and other countries to minimize costly roadway damages that occur in seasonally frozen areas during the annual spring thaw (Zarrillo et al., 2012). Concrete and asphalt become quite fragile from late winter as the ground begins to thaw. During the freezing season, sub-freezing air temperatures cause ice accumulation in the pavement structure (Baïz et al., 2008; Lachance-Tremblay et al., 2017; Lai et al., 2014) and subgrade soils (Liu and Yu, 2014; Lu et al., 2018; Yin et al., 2018). Thawing of the frozen ground begins on the surface as well as below the frozen layer in spring, e.g., March, April, and May in Michigan (Michigan Legislature Section 257.722). The resultant liquid water on top of the frozen layer may not efficiently drain out of the soil, as the surrounding soil remains frozen and impermeable (C-SHRP, 2000). The soil becomes temporarily saturated with water, appearing "spongy", and losses its strength to support the pavement, leading to thaw-weakening (Shoop et al., 2008; Simonsen and Isacsson, 1999; Xu et al., 2018). Paved roads with thin overlays may lose more than 50% of their bearing capacity in spring whereas a gravel road, built without sufficient base course thickness, may lose 70% (Isotalo, 1993). When trucks and heavy equipment travel over a layer of concrete or asphalt that is not well supported from beneath due to this thaw-weakening, cracks form and water is pumped through these cracks in the roadway (Marquis, 2008a). Thus, SLR and the associated pavement issues are closely related to the freeze-thaw cycles and the status of the pavement and subgrade soils.

Traditional SLR mainly depends on engineers' experience and visual observations in situ, such as water pumping from cracks in Maine (Marquis, 2008a). A survey (Kestler et al., 2000) of the practices of 45 state Department of Transportations (DOTs) and 3 forest service regional offices revealed that 45% of the agencies used inspection and observation to impose SLR, while 25% relied on a fixed date method.

* Corresponding author.
E-mail addresses: tbao@mtu.edu (T. Bao), zhenl@mtu.edu (Z. Liu), jpbland@mtu.edu (J. Bland).

https://doi.org/10.1016/j.coldregions.2019.102856
Received 26 November 2018; Received in revised form 10 March 2019; Accepted 5 August 2019
Available online 06 August 2019
0165-232X/

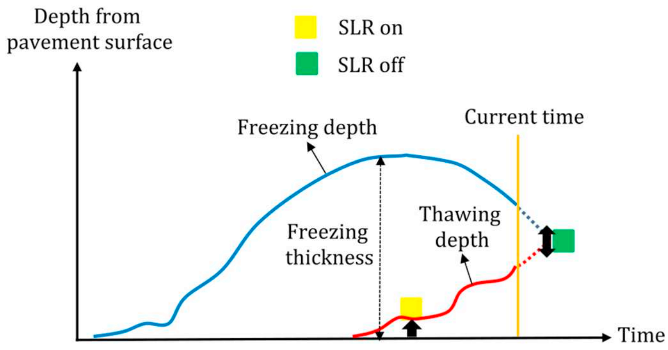

Fig. 1. SLR decisions based on freezing/thawing depth predictions (modified after (Baïz et al., 2008)).

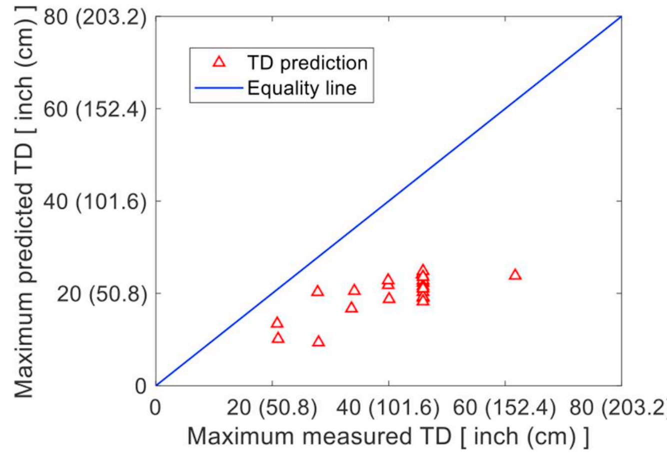

Fig. 2. Maximum predicted TDs vs measured TDs from measurement sites in Michigan (data is from (Baladi and Rajaei, 2015)).

57% of the agencies used inspection and observation to determine the removal date of SLR while 29% used a fixed date. In addition to the traditional methods, many agencies in the U.S. and Canada are trying to adopt quantitative SLR decision algorithms using the Freezing Depth (FD) and the Thawing Depth (TD) predicted based on the Freezing Index (FI) and/or the Thawing Index (TI). The first widely accepted analytical method was proposed by Mahoney et al. (1987) and McBane and Hanek (1986) for the state of Washington Department of Transportation (WDOT) and the Federal Highway Administration (FHWA). This first method involved FI and TI and set up a paradigm for later methods. Minnesota Department of Transportation (MnDOT) (Van Deusen et al., 1998) recommended applying SLR based upon a TI threshold of 25 °F-days (13.9 °C-days). Manitoba Department of Infrastructure and Transportation (MIT) in Canada (Bradley et al., 2012) recommended applying SLR at a TI threshold value of 27 °F-days (15 °C-days). MIT recommended an ending threshold set to no later than 56 days (8 weeks) from the start of SLR or when TI reaches 630 °F-days (350 °C-days). Currently, Baïz et al. (2008) suggested that the SLR placement corresponds to the time when the continuous thawing starts in the subgrade soils, as illustrated by the yellow square in Fig. 1. The SLR removal should take place after TD meets FD in the thawing season, i.e., the green square in Fig. 1, which was also adopted by Chapin et al. (2012).

In order to determine the placement and removal dates of SLR, accurate predictions of FD and TD, especially the latter one, are essential to prevent the extensive damage to the pavement due to the late placement or early removal of SLR. An unnecessarily long period for SLR will also cause an economic loss due to non-usage of the roads. For FD predictions, three major types of prediction models were widely utilized in the U.S. and Canada: the mechanistic model, the classic physico-empirical model, and the empirical model. The mechanistic models (Cluett et al., 2011; Fayer and Jones, 1990) were usually developed based on the physical process from a continuum mechanics perspective by considering heat transfer (Fourier's equation) and water movement (modified Richards' equation) in soils. The physico-empirical models, e.g., the Neumann' empirical model (Jiji and Ganatos, 2009), the Stefan's equation (Jiji and Ganatos, 2009), and the Modified Berggren equation (ACE-US, 1984; Aldrich and Paynter, 1953), were developed from the solution to a simplified case of the mechanistic model, in which FD is a function of the square root of FI and soil properties. The empirical models (Baïz et al., 2008; Tighe et al., 2007) further reduced the constraints by using FI only and lumping all the other terms in the physico-empirical models with suitable fitting constants.

For TD predictions, Chapin et al. (2012) demonstrated a prediction model based on the nonlinear regression analysis of field measurements, in which TD is a power function of TI. This power model, however, overlooked the physical process from a continuum mechanics perspective. Baïz et al. (2008) considered the physical process and predicted TD using exactly the same mathematical function (i.e., square root) and fitting constant numbers as those of FD based on TI and FI, in which two different TD models were developed, one for the freezing season and the other one for the thawing season. Efforts have also been made for predicting the maximum TD for the sites in Michigan using the Stefan's equation (Baladi and Rajaei, 2015). This Stefan's equation formulated TD as a square root of thermal properties of a pavement and its base/subbase soils, which thus shares the same mechanism when TD is a square root of TI. The maximum TD is very helpful to determine the removal of SLR (see Fig. 1). However, it is seen in Fig. 2 that the predicted maximum TDs in the existing study are significantly underestimated when compared to the measured TDs.

Despite the above progress, three key questions for predicting FD and TD still need to be addressed. First, most existing prediction models for TD use exactly the same mathematical formulation as that of FD. This, however, is site dependent and is not suitable for every case. The results in Fig. 2 clearly shows the large deviations of TD predictions for roadways in Michigan the same mathematical formulation for TD as that of FD is applied. Thus, a new TD prediction model is urgently needed to improve the TD prediction accuracy. Second, most existing prediction models, e.g., Chapin et al. (2012) and Baladi and Rajaei (2015), assume that FD can be predicted based on FI only (i.e., 2-dimensional line). In fact, FD is also highly correlated to TI (i.e., 3-dimensional surface) because intermittent thawing periods always exist in the freezing season. Baïz et al. (2008) included TI for predicting FD; however, FD in the freezing and thawing seasons is predicted separately using a piecewise function, which is inconvenient in practice. Therefore, no integrated FD and TD prediction model involving both FI and TI in the whole freeze-thaw cycle is available. Third, most existing prediction models, e.g., Baïz et al. (2008) and Chapin et al. (2012), are developed and validated against field data from only one or two sites due to the monetary and time constraints. Plenty of field data from 104 sites in Michigan alone are available, which have not yet been used.

To address the above questions, in this study, we propose a new multivariate FD/TD prediction model, which is easily implementable for supporting SLR decision-making. The proposed model is primarily evaluated using field data measured at five typical sites in Michigan. The evaluation results for FD and TD based on both FI and TI in a 3-dimensional space are presented and discussed.

2. Theory and method

2.1. Field measurements

Michigan Department of Transportation (MDOT) deployed a Road Weather Information System (RWIS) to measure road and weather conditions on highways and communicate this information to users in a

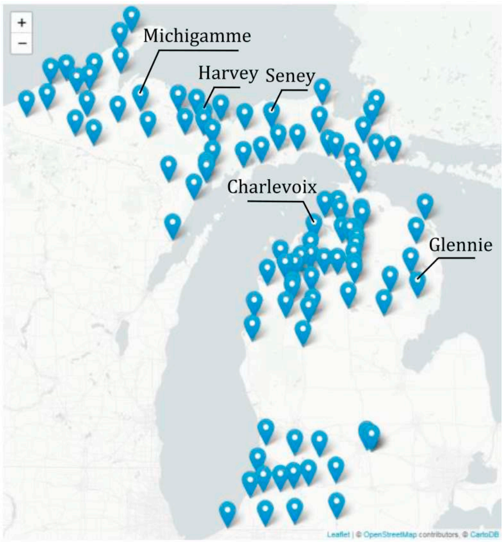

Fig. 3. Overview of monitored sites with ESSs in Michigan.

maintenance facility. Through a series of strategically placed Environmental Sensor Stations (ESSs) in the RWIS, key road and weather conditions (e.g., humidity, wind speed, average air temperature, and temperatures of the pavement surface and subsurface) are measured in real-time. To share yearly RWIS data in public, we developed the MDOT SLR website (https://mdotslr.org/). As of now, there are 104 sites implemented with ESSs in Michigan as shown in Fig. 3. The RWIS data for these sites can be freely downloaded from the MDOT SLR website.

In this study, we primarily selected five typical sites for analyses, three from the Upper Peninsula and two in the Lower Peninsula.

The pavement structure of the five selected sites primarily consists of an asphalt/concrete surface, a granular base, and a soil sub-base. Details of the pavement structure, soil types, and properties can be found in Baladi and Rajaei (2015). Table 1 shows all the measured temperatures needed for this study. The air temperature was measured by the air temperature sensor, while the pavement surface and base temperatures were measured by surface and subsurface sensors, respectively. For base temperatures, 15 subsurface sensors were used to measure the temperatures from the base surface to a depth of 72 in. (1.83 m), which can be used to calculate FD and TD.

2.2. A new freezing-thawing depth prediction model

Calculations of FD and TD are related to the solution to a phase-change (ice-liquid) problem of heat transfer. In a pioneering study, Neumman solved FD by analyzing the 1D heat transfer in a semi-infinite soil (Jiji and Ganatos, 2009). FD in the Neumman's equation is a function of the surface temperature, time, and thermal conductivities of both the frozen and unfrozen soils (see details in Baladi and Rajaei (2015)). A special case of the Neumman's equation was further solved by assuming no heat transfer in the liquid (Baladi and Rajaei, 2015), in which FD is formulated by

$$FD = \sqrt{\frac{2\lambda_f}{\rho l}(T_0 - T_{s,s})t} \tag{1}$$

where λ_f is the thermal conductivity of a frozen soil (W/(m °C)), ρ is the soil density (kg/m^3), l is the latent heat of fusion (J/kg), T_0 is the freezing point of bulk water (= 0 °C), $T_{s,\,s}$ is the soil surface temperature, and t is the time (day). Based on Eq. (1), many physico-empirical models were further developed. These physico-empirical models share a common form of Eq. (2) to calculate FD (Aldrich and Paynter, 1953)

$$FD = a_o\sqrt{\frac{48\lambda_f nFI}{L}} \tag{2}$$

where L is the volumetric latent heat of fusion (J/m^3), n is a dimensionless parameter converting the air temperature index to the surface temperature index, a_o is a dimensionless correction factor considering the initial freezing depression (Berg et al., 2006).

The recent physico-empirical models (Asefzadeh et al., 2016; Baïz et al., 2008; Marquis, 2008b; Miller et al., 2012) further loosened the constraints in Eq. (2) by only keeping FI and lumping all the other terms with physical meanings into one or two fitting constants. The fitting constants can be obtained by linear regression with measured data. Therefore, the physico-empirical models are also statistical models. One major feature of these physico-empirical models is the linear relationship between FD and the square root of FI. The above existing studies have proved that satisfactory predictions for FD can be made using the square root of FI. This study also uses this method for the FD prediction with the square root of FI. In addition, results from the field measurements for the five selected sites and additional sites, shown in Fig. 4, clearly indicate that FD follows a square root function decay as TI increases.

Considering the above facts, the following model is proposed for FD involving both FI and TI

$$FD = a\sqrt{FI} + \sqrt{c - bTI} + d \tag{3}$$

where a, b, c, and d are fitting constants, the first three always positive. It is known that freezing and thawing processes are similar (Konrad, 1989); as a result, the mathematical formulations for TD and FD are similar

$$TD = -e\sqrt{FIT} - \sqrt{g - fTI} + h \tag{4}$$

where e, g, f, and h are fitting constants, the first three always positive. FIT is the cumulative freezing index in the thawing period only. FI is not adopted here for TD, as FI mainly represents the cumulative frost in the pavement base during the freezing period, which in fact is irrelevant to TD. Therefore, FIT is adopted, which can appropriately consider the cumulative freezing index when the thawing starts. The fitting constants for FD and TD reflect the real situation for the depth and duration of the freeze and/or thaw penetration in the pavement base. The fitting constants can be obtained using the nonlinear least squares method on each site. It is noted that $c - bTI > 0$ and $g - fTI > 0$ should be ensured (i.e., the principal square root of a positive number) in the nonlinear regression analysis.

The cumulative freezing index during the freezing period can be calculated based on $T_0 = 0$°C over a given period

Table 1
Needed parameters for analyses.

Material	Measured temperature															
Air	Average temperature (°C)															
Pavement	Surface temperature (°C)															
	Base temperature (°C)	Depth from base surface (inch)														
		0	3	6	9	12	18	24	30	36	42	48	54	60	66	72

Note: 1 in. = 2.54 cm.

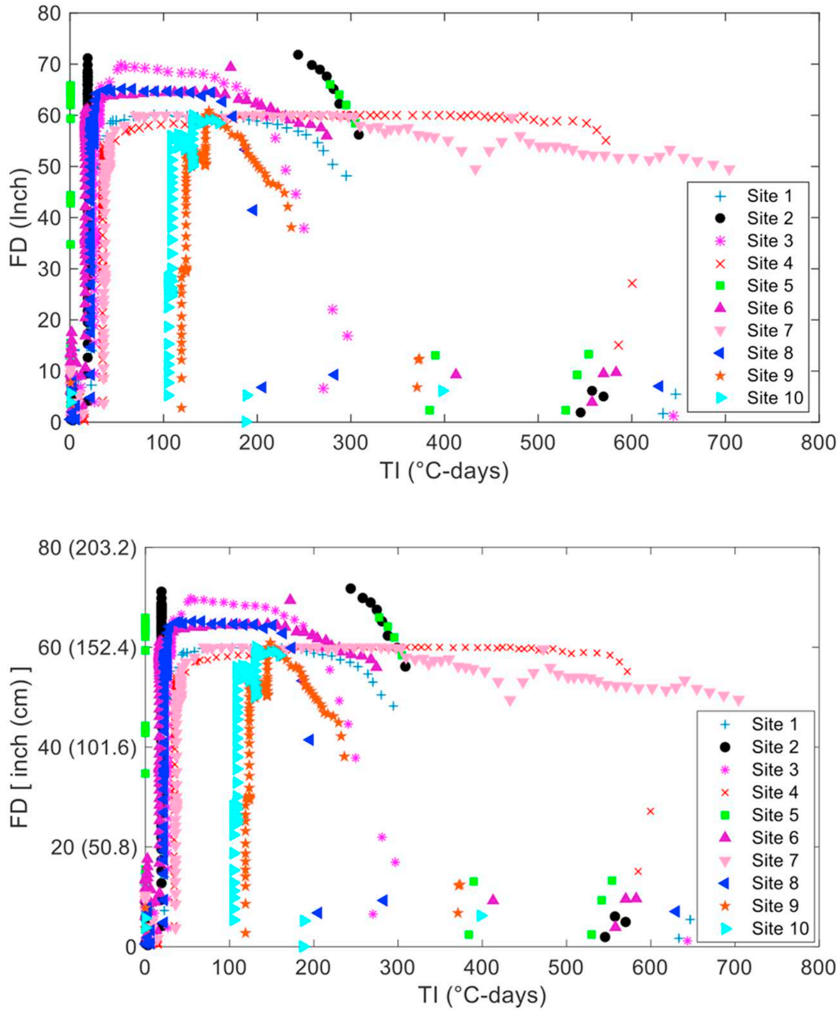

Fig. 4. Field measurement results of TI-FD relationships from ten sites in Michigan.

$$\{FI = \sum (T_0 - T_s), T_0 - T_s < 0 \Rightarrow T_0 - T_s = 0 \tag{5}$$

where T_s is the pavement surface temperature. Similarly, FIT can be calculated using Eq. (5) starting from the date when the first TD occurs in the thawing period. The cumulative thawing index is computed by

$$\begin{cases} TI = \sum (T_s - T_{ref}) \\ T_s - T_{ref} < 0 \Rightarrow T_s - T_{ref} = 0 \end{cases} \tag{6}$$

where T_{ref} is the reference temperature to account for the amount of solar radiation and thermal properties of the pavement material. In this study, $T_{ref} = -1.67$°C was used according to the guideline of FHWA-WSDOT (Mahoney et al., 1987). Eqs. (5)–(6) use the pavement surface temperature instead of the average air temperature. This is due to the fact that FI and TI calculated with the average air temperature failed to correlate FD and TD in the freeze-thaw cycle (see Fig. 13), which will be discussed later in detail.

2.3. Model implementation for SLR

In general, agencies require a notice at least 5 days prior to the placement and removal of SLR. To apply the FD/TD prediction model to practical SLR decision-making, Fig. 5 presents a brief flowchart suggesting how this could be done. Based on the real-time field data, FD and TD can be calculated. When the thawing starts and TD continuously increases to a predefined threshold, SLR can be set (see Fig. 1). SLR will be removed when FD meets TD or reaches other pre-specified thresholds. The decision to remove SLR can be easily made by observing the FD and TD graphs obtained by the prediction model. At each site, SLR decisions can be made based on the present FD/TD prediction models.

3. Results

3.1. Air and pavement surface temperature

The daily average air temperature and daily pavement surface temperature for the five selected sites are presented in Fig. 6, which shows the measurements from August 1st 2017 to June 1st 2018 covering the entire freeze-thaw cycle. The pavement surface temperature in general is greater than the average air temperature, in particular for the periods before October 2017 and after April 2018. It is also seen that the pavement surface temperature tends to be below 0 °C starting from the middle of November 2017 for all the sites, while it tends to be above 0 °C starting from March 2018. This indicates that freezing likely starts in the pavement layers from the middle of November 2017 and thawing likely begins occurring from March 2018 for all the selected sites. In Fig. 6c, the data for the site Seney are missing from September 26th 2017 to November 14th 2017, probably due to the lost connection between the sensors and the ESS at the site during the data transmission. However, the missing data have a negligible effect because the complete freeze-thaw cycle is included in the collected data in Fig. 6c.

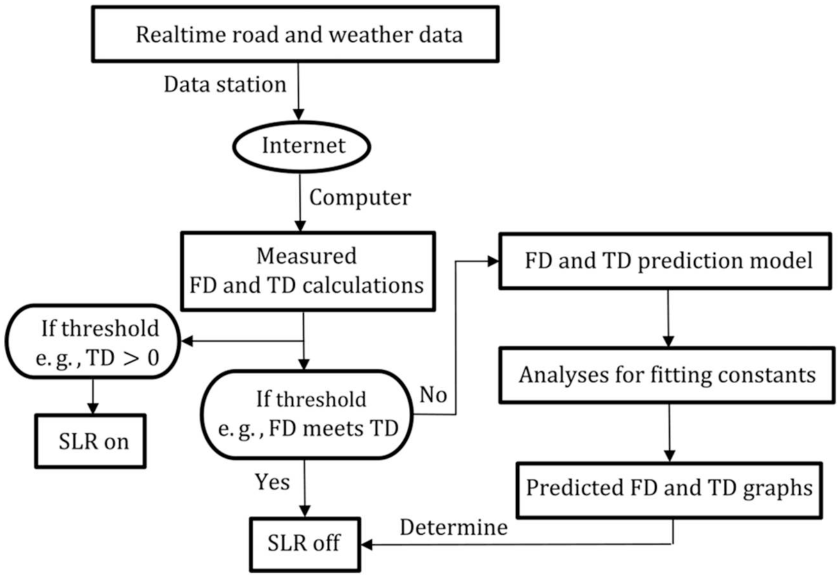

Fig. 5. Conceptual flowchart of the FD/TD prediction model implementation for SLR.

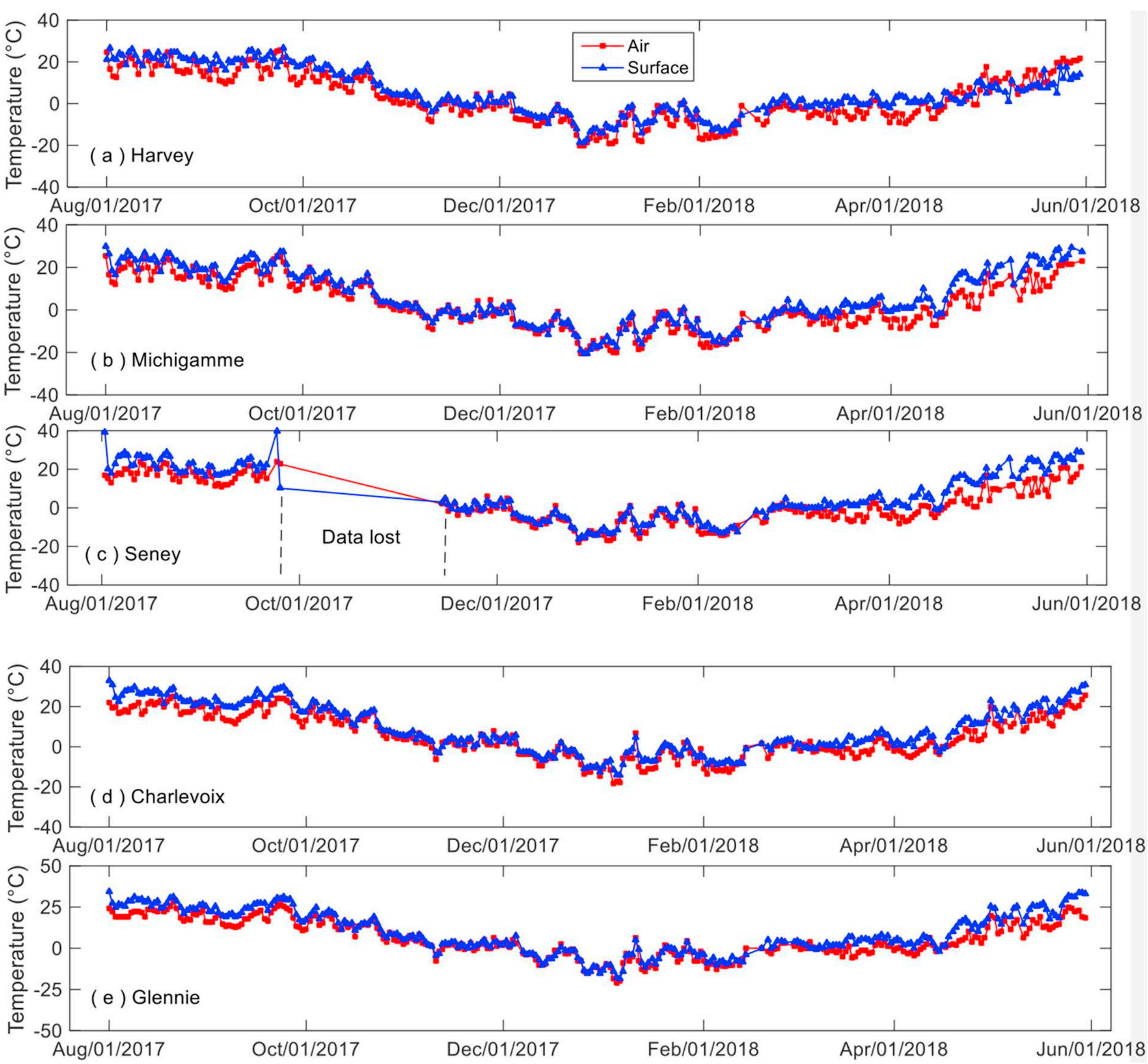

Fig. 6. Average air temperatures and pavement surface temperatures for the five selected sites.

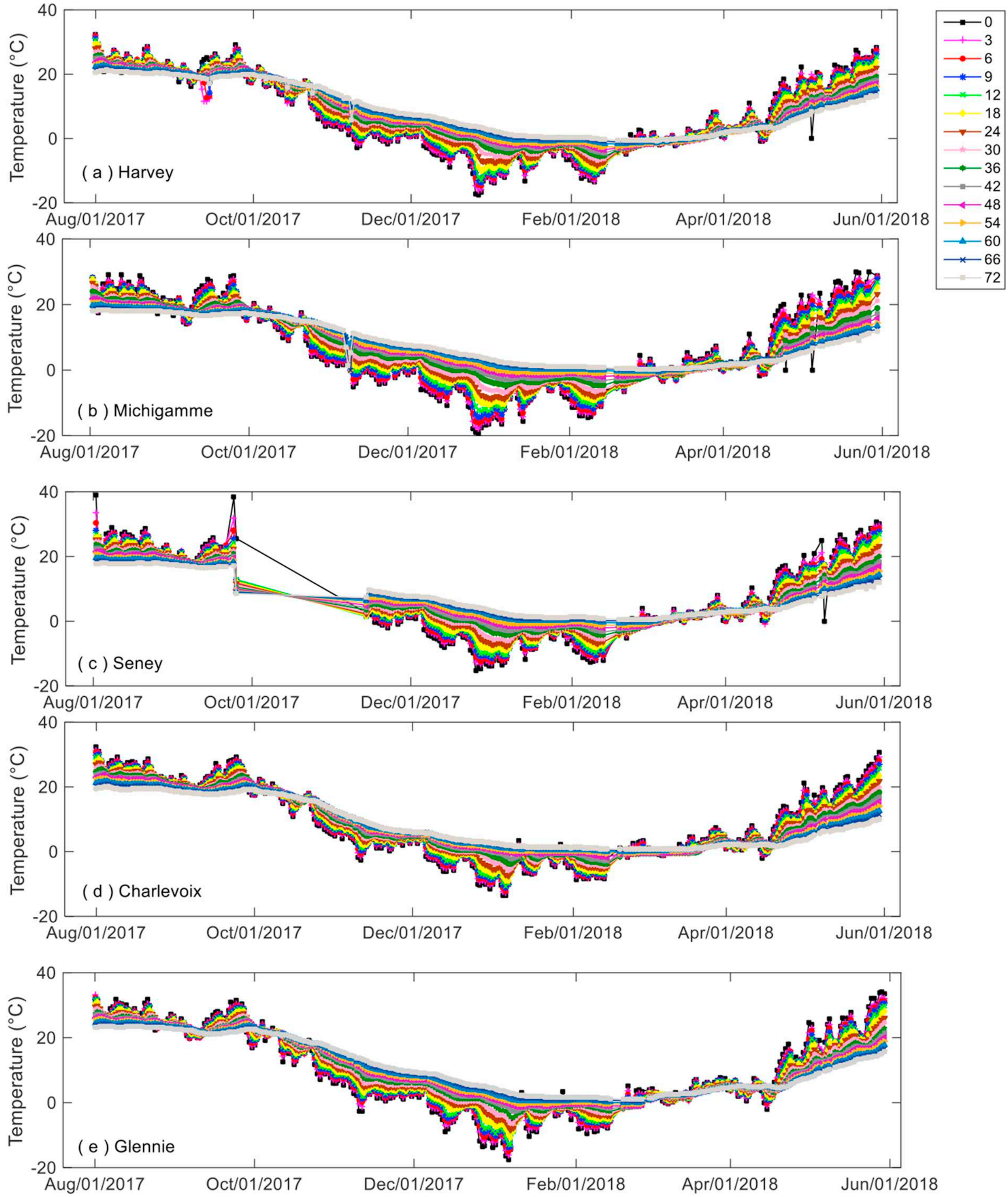

Fig. 7. Pavement base temperatures for the five selected sites.

3.2. Base temperature

The base temperature reflects the freezing and thawing penetration of the base and is used to determine FD and TD in the pavement layers. Fig. 7 shows the measured base temperatures for all 15 locations from 0 to 72 in. (0–1.83 m) in Table 1. Similar to the air temperature and the pavement surface temperature in Fig. 6c, the base temperature data collected at the site Seney are not available from September 26th 2017 to November 14th 2017. It can be clearly seen in Fig. 7 that from the middle of November 2017 to March 2018, the temperature measured in the base layer at different depths increases as the depth increases for all the sites. Among them, the measured temperatures at the bases, whose depths are less than 24 in. (60.96 cm), are below 0 °C. Starting from March 2018, the reverse temperature trend is observed, especially after April 2018, where the measured temperature decreases as the depth increases. These observations further confirm that for these sites, the thawing period starts around the beginning of March 2018. The freezing period is from the middle of November 2017 to the end of February 2018.

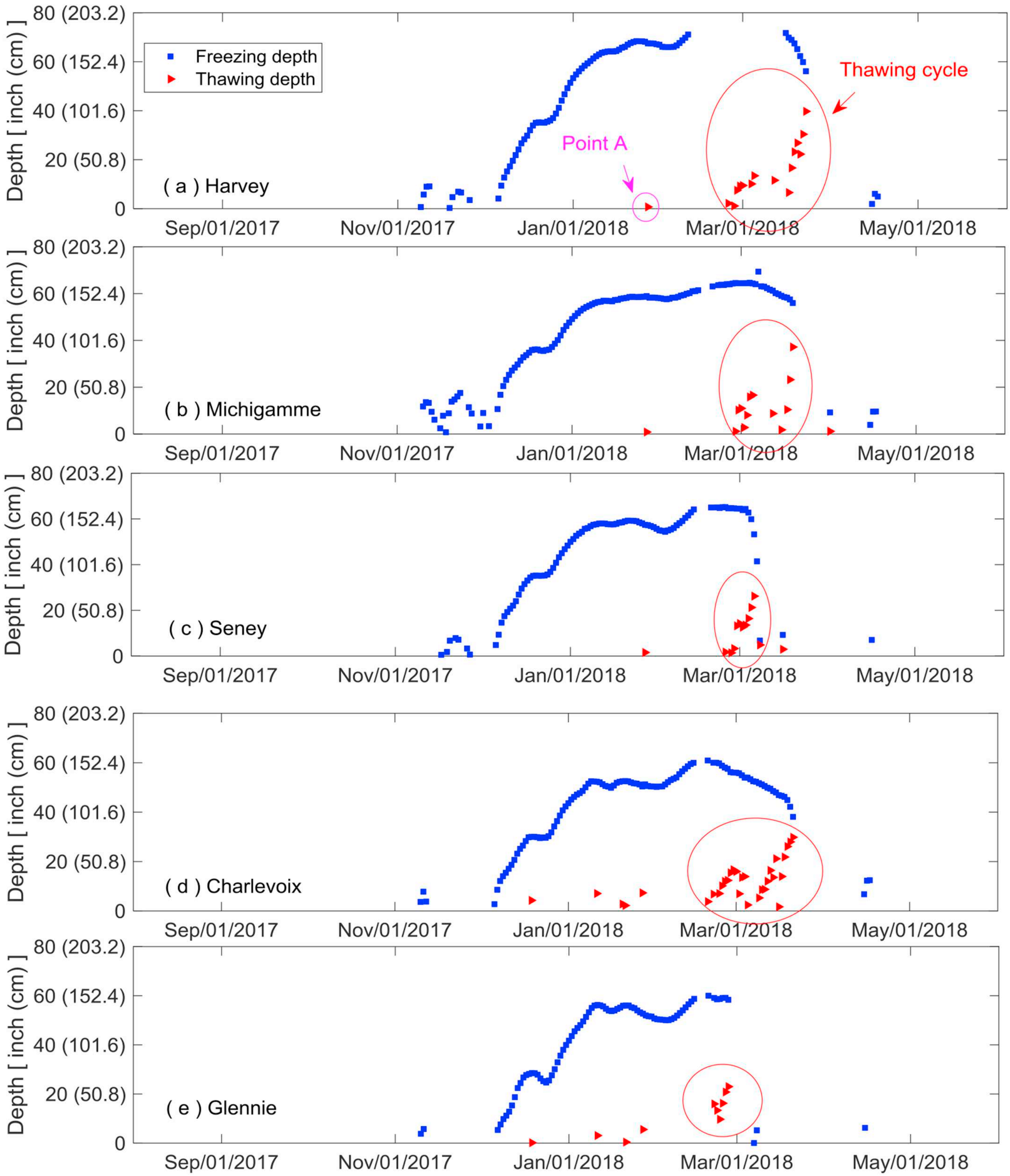

Fig. 8. Calculations of measured FDs and TDs for the five selected sites.

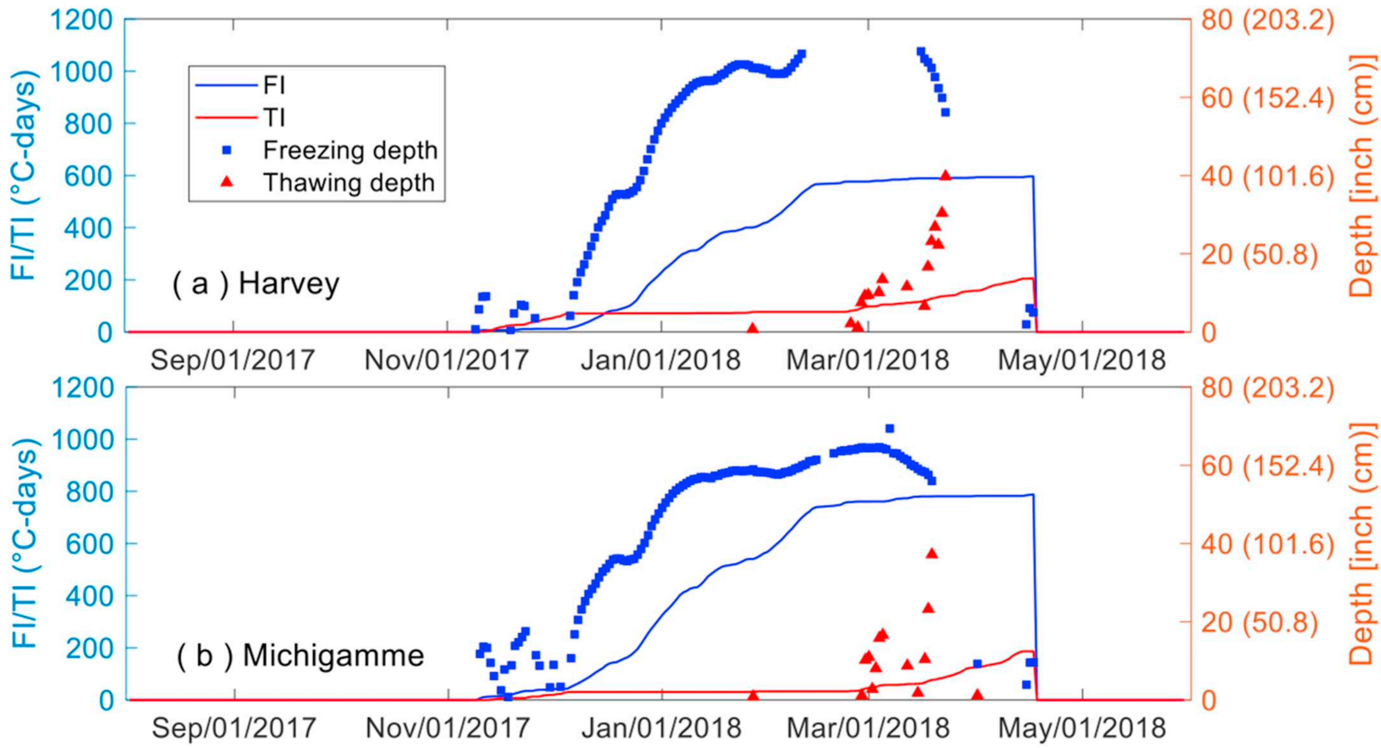

Fig. 9. FI/TI calculated with the pavement surface temperature: (a) Harvey and (b) Michigamme.

3.3. Freezing and thawing depths

FD and TD for the five selected sites can be calculated based on the base temperatures in Fig. 7. For this purpose, two adjacent base temperatures from 0 to 72 in. (0–1.83 m) were compared. FD occurs if the previous base temperature is negative and the next one is positive, while TD appears if the previous base temperature is positive and the next one is negative. To calculate FD and TD, linear interpolation was used and the base surface (i.e., base depth = 0) was assumed as a datum. All calculated FDs and TDs below the datum are positive. The measured FDs and TDs for the five selected sites are presented in Fig. 8. We can see that FD occurs around the middle of November 2017 and starts decreasing significantly at the beginning of March 2018, which corresponds to the freezing and thawing starting dates seen in Fig. 7. During the freezing period, FD decreases somewhat, especially at the beginning of the freezing period. This is because there were several warm days to thaw the pavement base, leading to a decrease in FD.

For all the sites, TD increases starting from March 2018, which agrees well with Fig. 7. However, there are a few TD points before March 2018, e.g., Point A in Fig. 8a. This could be because of some warm days during the freezing period. For some sites, as shown in Fig. 8b and Fig. 8c, there are also a few TD points when one freeze-thaw cycle is complete, where FD meets TD. This is again due to some warm days after the freeze-thaw cycle ends.

3.4. Freezing and thawing indices

The pavement surface temperature was used in this study to calculate FI and TI. The reason for using the pavement surface temperature will be discussed in detail in Section 4.1. Taking the Harvey and Michigamme sites for example, Fig. 9 shows the variations of FI and TI for these two sites, in which the corresponding FD and TD are also plotted. FI and TI were calculated starting from the first FD and ending by the last FD or TD. The rest of FI and TI were treated as zero.

3.5. Freezing-thawing depth model evaluation

FDs and TDs presented in Fig. 8 for all the selected sites were used for the statistical analyses based on the proposed model using FI and TI values calculated with the pavement surface temperature. Fig. 10a shows the fitting result of FD for Harvey. A curving surface for predicted FD is exhibited, in which FD increases as FI increases and decreases as TI increases. The maximum FD could be obtained when FI almost remains unchanged and TI significantly increases. The predicted FD surface is in good agreement with the measured FDs and the coefficient of determination is found to be 0.94. Therefore, the proposed FD model performs well in predicting FD with the high accuracy.

Fig. 10b presents the surface fitting result of TD formulated by TI and FIT for Harvey. We can clearly see that the predicted TD surface is very close to the measured TDs. TD increases with an increase in TI. However, it is difficult to observe how TD changes with FIT from Fig. 10b, as Point A does not belong to TD data in the thawing period. This point appears before February 2018 due to the occurrence of some warm days in the freezing period (see Fig. 8a). As our goal is to predict TD in the thawing period for applying SLR, Point A beyond the thawing cycle in Fig. 8a can be removed. It can be seen in Fig. 10c that TD decreases as FIT increases when Point A is excluded. The predicted TD surface fitted to the measured TDs in the thawing cycle becomes more accurate and the coefficient of determination increases from 0.83 to 0.90 accordingly.

For the other four sites, Fig. 11 presents the 3-dimensional fitting surfaces of FD and TD. The TD data in the thawing cycle in Fig. 8 were

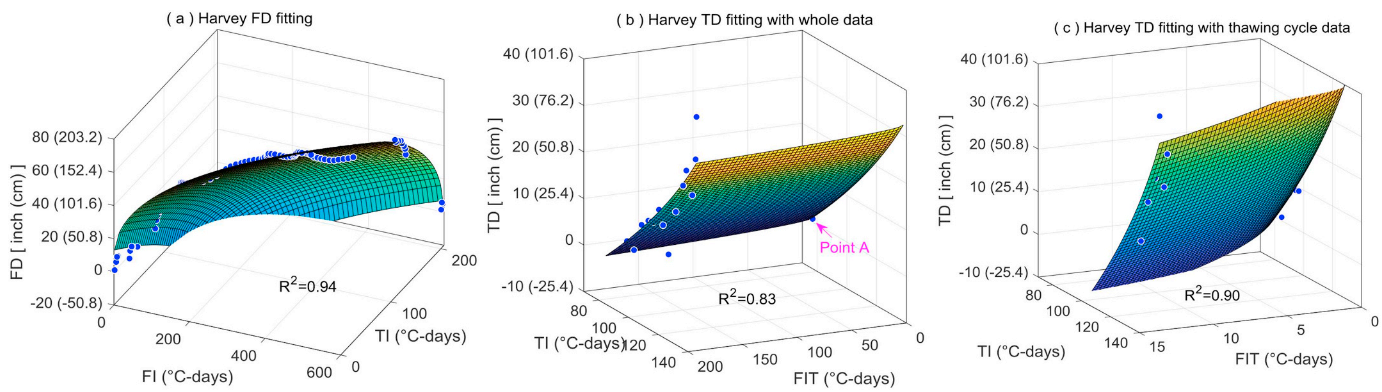

Fig. 10. Fitting surfaces for Harvey: (a) FD fitting, (b) TD fitting with the whole TD data, (c) TD fitting with the thawing cycle data.

used for fitting TD for each site. It can be seen that the predicted FD surfaces for these sites match well with the measured FDs. The coefficient of determination for most sites is found to be as high as 0.93. For TD predictions, the predicted TD surfaces for Michigamme and Glennie are in good agreement with the measured TDs (see Fig. 11a and d). The predicted TD surfaces for the other two sites are not as good as those for Harvey and Michigamme, as shown in Fig. 11b and c. The reason is that the measured TDs do not increase continuously, but rather, go up and down, for example, Charlevoix in Fig. 8c. This makes it difficult to fit a 3-dimensional surface in the nonlinear regression analysis. However, the predicted TD surfaces for these two sites capture the key mechanism of the TD-TI-FIT relationship, i.e., TD nonlinearly increases with an increase in TI and a decrease in FIT. Also, from the fitting constants tabulated in Table 2, each fitting constant has the same sign for all the selected sites, regardless of FD and TD predictions. This implies that the FD-FI-TI relationship for all the five selected sites has the same trend, so is that of the TD-TI-FIT relationship. The proposed model was further assessed by additional sites shown in Fig. 12. The 3-dimensional fitting surfaces for these additional sites are very similar to those in Fig. 11. The fitting results for these additional sites are tabulated in Table 3. It is seen that the coefficient of determination for FD and TD for most sites is higher than 0.8, which further confirms that the proposed model is adaptable to other sites. The above evaluation results clearly show the key varying mechanisms of both the FD-FI-TI relationship and the TD-TI-FIT relationship, and also demonstrate the high accuracy of the proposed model for predicting FD and TD for most sites.

4. Discussion

4.1. Calculations of FI and TI via surface temperature rather than air temperature

Calculations of FI and TI are needed to accurately predict FD and TD. To obtain appropriate FI and TI, the pavement surface temperature was used in this study. This is different from most existing models (e.g., Baïz et al. (2008) and Chapin et al. (2012)) that adopt the average air temperature to calculate FI and TI. To illustrate the advantage of using the pavement surface temperature, Fig. 13 shows the comparisons of FI and TI calculated with the pavement surface temperature and those calculated with the average air temperature for Harvey and Michigamme, in which the corresponding FD and TD are also plotted.

It is clearly seen in Fig. 13 that when the thawing starts from March 2018, FI calculated with the average air temperature (dashed blue line) still increases. At the same time, FD significantly decreases and TD continuously increases. Starting from March 2018, it is also seen that TI calculated with the air temperature (dashed red line) almost remains unchanged, which does not appear reasonable. When the thawing starts, TI should increase accordingly and FI should decrease, as the increase in TD is mainly attributed to the continuous thaw penetration in the pavement base. This causes the accumulated frost in the base to thaw and accordingly, FD should decrease significantly. FI and TI calculated with the air temperature, however, fail to match the changes in TD and FD in a realistic way. When the pavement surface temperature is applied, as shown in Fig. 13, FI (solid blue line) almost remains unchanged and TI (solid red line) increases starting from March 2018, which matches very well with the corresponding changes in TD and FD. In addition to the above two sites, FI and TI calculated with the pavement surface temperature for the rest of the three sites also match quite well with the trends of FD and TD, which can be found in the Appendix. Therefore, the pavement surface temperature is more suitable to calculate FI and TI for predicting FD and TD than the average air temperature.

4.2. Prediction improvement

Good predictions for both FD and TD, especially the latter one, can be obtained with the proposed model. The 3D fitted surfaces hide the underneath measured data, causing a difficulty in visually evaluating the prediction accuracy. To clearly see the predictions, taking the Harvey site for example, Fig. 14 shows the fitted line instead of fitted surfaces for both FD and TD. We can see in Fig. 14 that the fitted line for FD agrees well with the measured FDs in a 3D space. The fitted line for TD in Fig. 14b is also very close to the measured TDs, in which the "staircase shape" is observed. This is due to the fact that TI keeps unchanged and in the meantime FIT increases if there have a few freezing days during the thawing period, and vice versa.

The good predictions with the proposed model are primarily attributable to three reasons. First, the pavement surface temperature is used to reflect more realistic pavement thermal conditions than the air temperature, as explained in Section 4.1. Second, the proposed model adopts the mathematical form of $-\sqrt{g - fTI}$ for TD predictions rather than the general form of $f\sqrt{TI}$ used in the existing studies (e.g., Baïz et al. (2008)). The latter one may be only suitable for a specific site, while the former one has been confirmed by many different sites shown in Fig. 12. Third, the proposed model adopts FIT rather than FI for predicting TD. The selection of FIT is more reasonable because the value of FI also determines the TD prediction accuracy in addition to its mathematical form (i.e., square root). Therefore, FIT is better than FI

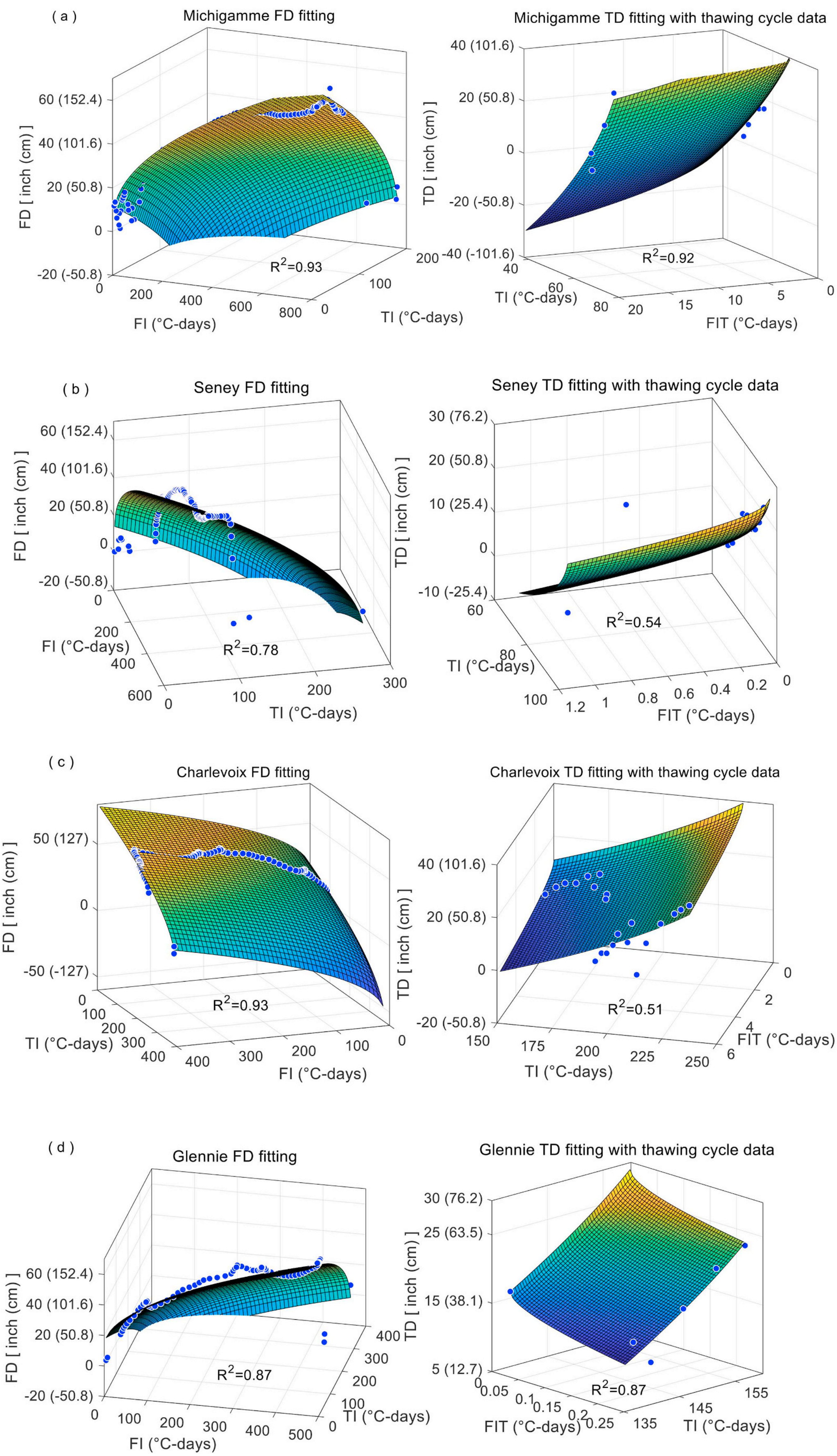

Fig. 11. Fitting surfaces for FD and TD: (a) Michigamme, (b) Seney, (c) Charlevoix, and (d) Glennie.

Table 2
Fitting results for the five selected sites.

Site	Variable prediction	Fitting constant				
		unit: inch °C-day$^{-0.5}$	inch^2 °C-day^{-1}	inch^2	inch	
Harvey	FD	*a*	*b*	*c*	*d*	R^2
		4.03	69.24	14,574	−109.5	0.94
	TD	*e*	*f*	*g*	*h*	R^2
	TD with whole data	0.17	56.59	1717.91	71.9	0.83
	TD with thawing cycle	5.11	120.3	18,422.1	94.93	0.9
Michigamme	FD	*a*	*b*	*c*	*d*	R^2
		2.56	36.84	6913.6	−78.34	0.93
	TD with thawing cycle	*e*	*f*	*g*	*h*	R^2
		6.31	229.7	19,071	100.1	0.92
Seney	FD	*a*	*b*	*c*	*d*	R^2
		2.67	29.06	8028.8	−78.81	0.78
	TD with thawing cycle	*e*	*f*	*g*	*h*	R^2
		8.16	50.8	5410.8	42.27	0.54
Charlevoix	FD	*a*	*b*	*c*	*d*	R^2
		3.15	17.09	528.36	−65.47	0.93
	TD with thawing cycle	*e*	*f*	*g*	*h*	R^2
		5.43	29.03	1126.04	69.2	0.51
Glennie	FD	*a*	*b*	*c*	*d*	R^2
		3.60	39.78	215.31	−64.56	0.87
	TD with thawing cycle	*e*	*f*	*g*	*h*	R^2
		11.90	35.69	688.92	51.99	0.87

Note that 1 in. = 2.54 cm.

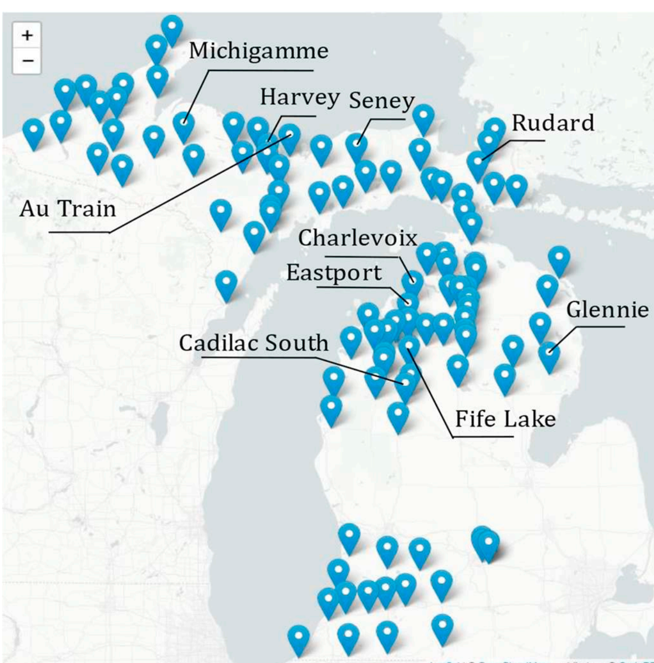

Fig. 12. Locations of additional sites in Michigan.

Table 3
Prediction results for additional sites.

Site	Variable prediction	Fitting constant				
		unit: inch °C-day$^{-0.5}$	inch^2 °C-day^{-1}	inch^2	inch	
Rudyard	FD	*a*	*b*	*c*	*d*	R^2
		2.36	7.08	2790.05	−69.93	0.96
	TD with thawing cycle	*e*	*f*	*g*	*h*	R^2
		1.19	20.30	2033.04	83.42	0.83
Eastport	FD	*a*	*b*	*c*	*d*	R^2
		3.37	13.39	460.14	−65.84	0.83
	TD with thawing cycle	*e*	*f*	*g*	*h*	R^2
		0.56	70.37	1339.69	68.11	0.80
Au Train	FD	*a*	*b*	*c*	*d*	R^2
		3.16	51.25	427.50	−76.16	0.84
	TD with thawing cycle	*e*	*f*	*g*	*h*	R^2
		2.70	11.11	204.37	36.92	0.54
Cadillac South	FD	*a*	*b*	*c*	*d*	R^2
		0.83	0.91	233.98	−13.39	0.87
	TD with thawing cycle	*e*	*f*	*g*	*h*	R^2
		0.32	1.70	210.58	22.88	0.85
Fife Lake	FD	*a*	*b*	*c*	*d*	R^2
		3.80	27.25	383.19	−90.74	0.92
	TD with thawing cycle	*e*	*f*	*g*	*h*	R^2
		11.00	23.10	388.24	58.94	0.84

1 in. = 2.54 cm.

for the TD prediction by appropriately considering the cumulative freezing index when the thawing starts.

Though the FD and TD predictions are promising for most sites in this study, there are still deviations for a few sites, e.g., Seney in Fig. 11b. The possible reason is that factors, such as solar radiation and thermal properties of pavement materials, are not considered directly, but instead, considered via a constant T_{ref}. The effect of the solar radiation is believed to be significant as the solar radiation can significantly change both the pavement surface and air temperatures. However, the proposed model can predict both FD and TD with a high accuracy for most sites even using a constant T_{ref}. Fig. 15 presents the comparison between the previous TD predictions (Baladi and Rajaei, 2015) in Michigan and those with the proposed model. In addition to the selected five typical sites, three additional sites were also analyzed to evaluate the predicted maximum TDs. We can clearly see that the TD predictions in this study are very close to the measured TDs and much better than the previous TD predictions (Baladi and Rajaei, 2015). Therefore, the TD predictions have been significantly improved.

5. Conclusions

This study proposes a new multivariate model for predicting FD and TD to support SLR decision-making. The model can give a curving surface of FD and TD in a 3-dimensional space by considering both the freezing and thawing indices. For the model evaluation, yearly field data measured at five typical sites from 104 sites in Michigan were used. The results indicated that the use of the pavement surface temperature gives reasonable FI and TI and better results than the average

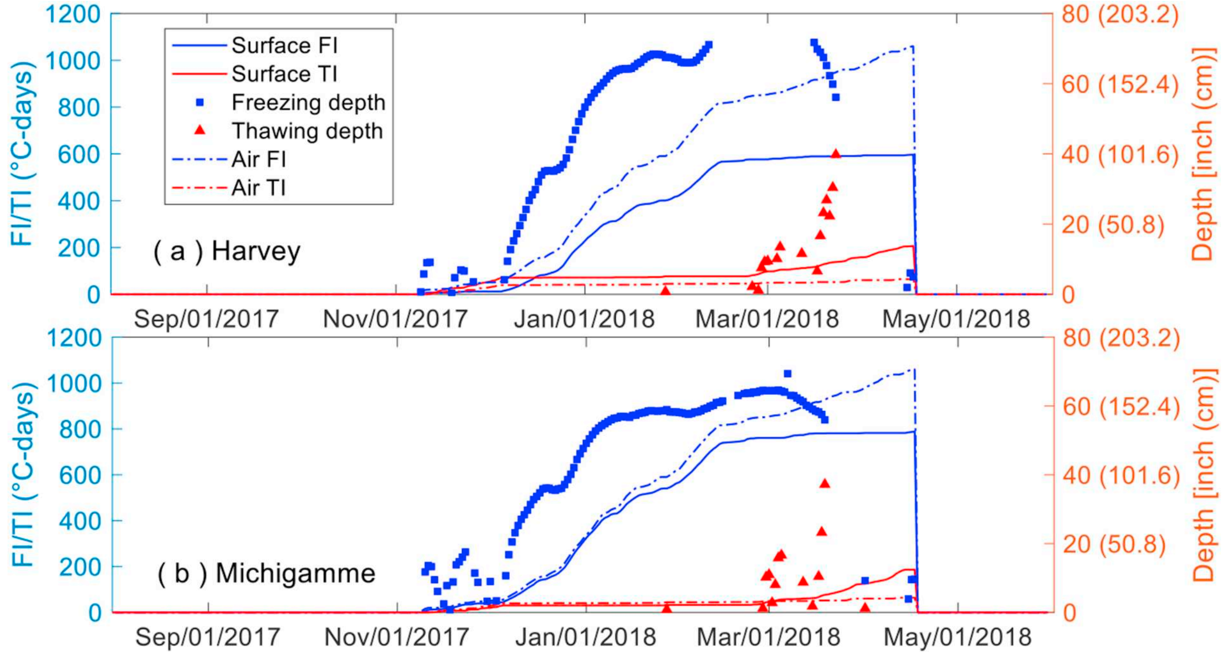

Fig. 13. Comparisons of FI/TI calculated with the pavement surface temperature and the average air temperature: (a) Harvey and (b) Michigamme.

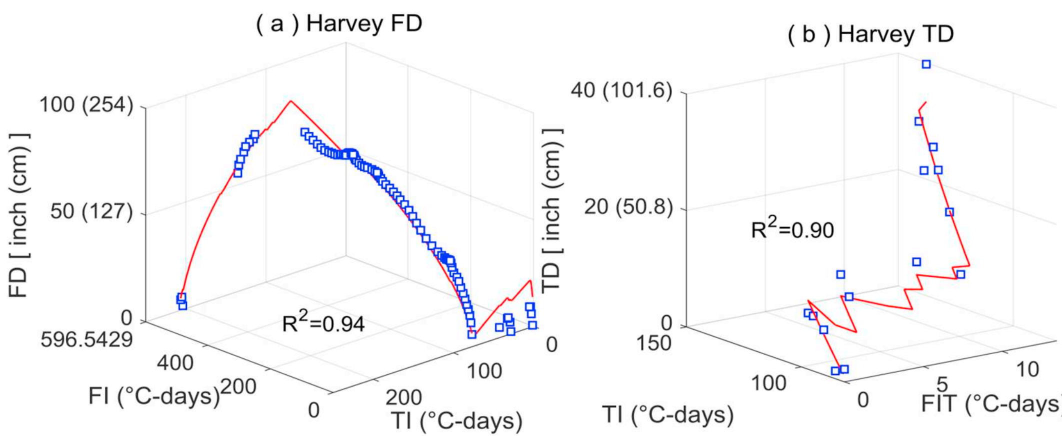

Fig. 14. Fitting lines for Harvey: (a) FD fitting, (b) TD fitting with the thawing cycle data.

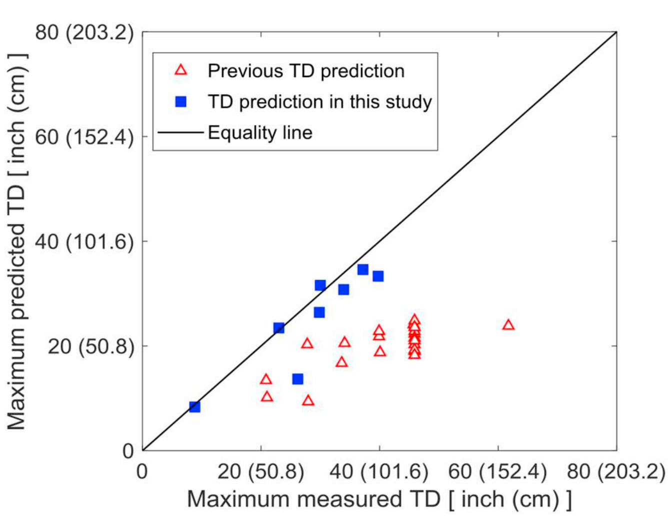

Fig. 15. Comparison of the maximum measured TDs and predicted TDs.

air temperature. FI and TI calculated with the pavement surface temperature match well with the corresponding changes in FD and TD with time. Therefore, the pavement surface temperature is more appropriate to calculate FI and TI for FD and TD predictions.

Evaluation of the results from the proposed model revealed that FD can be predicted with high accuracy for all the selected sites. For the FD-FI-TI relationship, the 3-dimensional surface clearly demonstrated that FD increases as FI increases and decreases as TI increases in the freeze-thaw cycle. The predicted TDs for three selected sites are very close to the measured TDs. There are deviations in the TD predictions for the other two sites, which is possibly due to the fact that factors, e.g., solar radiation and thermal properties of pavement materials, are not considered directly during the thawing period. However, the TD predictions have been significantly improved when compared to the previous TD predictions. Therefore, the proposed model is a capable tool for practice for roadways in cold regions in support of SLR decision-making. In addition, the present study provides field data that have not been reported earlier in the literature and that can be used for validating other prediction models.

Acknowledgments

This research is supported by the Michigan Department of Transportation (MDOT OR 16-009). The authors also thank V. R. (Sivan) Parameswaran (Retired Senior Guest Researcher, National Research Council Canada, Ottawa, Ontario) for his suggestions and edits.

Appendix A. Appendix

Fig. A.1 presents FI and TI values calculated with the pavement surface temperature for Seney, Charlevoix, and Glennie.

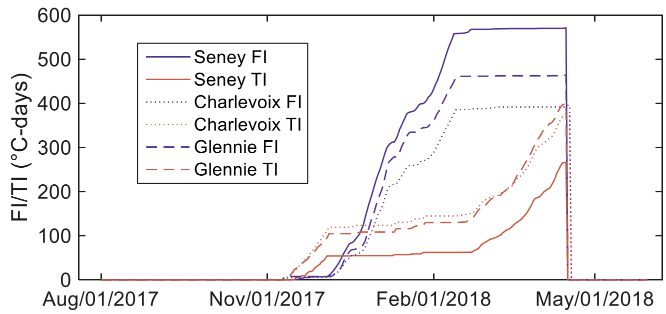

Fig. A.1. FI and TI for Seney, Charlevoix, and Glennie.

References

ACE-US, 1984. Pavement criteria for seasonal frost conditions. In: EM 1110-3-138, Department of the Army Technical Manual. U.S. Army Corps of Engineers.
Aldrich, H.P.J., Paynter, H.M., 1953. Analytical Studies of Freezing and Thawing of Soils. Arctic Construction and Frost Effects Lab, Boston, MA.
Asefzadeh, A., Hashemian, L., Haghi, N.T., Bayat, A., 2016. Evaluation of spring load restrictions and winter weight premium duration prediction methods in cold regions according to field data. Can. J. Civ. Eng. 43 (7), 667–674.
Baïz, S., Tighe, S., Haas, C., Mills, B., Perchanok, M., 2008. Development of frost and thaw depth predictors for decision making about variable load restrictions. Transportation Research Record: Journal of the Transportation Research Board (2053), 1–8.
Baladi, G.Y., Rajaei, P., 2015. Predictive Modeling of Freezing and Thawing of Frost-Susceptible Soils. Michigan State University, Department of Civil & Environmental Engineering, Lansing, MI.
Berg, R.L., Kestler, M.A., Eaton, R.A., Benda, C.C., 2006. Estimating when to apply and remove spring load restrictions. In: Current Practices in Cold Regions Engineering. American Society of Civil Engineers, Orono, Maine, USA, pp. 1–11.
Bradley, A., Ahammed, M., Hilderman, S., Kass, S., 2012. Responding to climate change with rational approaches for managing seasonal weight programs in Manitoba. In: Cold Regions Engineering 2012: Sustainable Infrastructure Development in a Changing Cold Environment, pp. 391–401.
Chapin, J., Kjartanson, B.H., Pernia, J., 2012. Comparison of two methods for applying spring load restrictions on low volume roads. Can. J. Civ. Eng. 39 (6), 599–609.
Cluett, C., Gopalakrishna, D., Middleton, D., 2011. Clarus multi-state regional demonstrations, evaluation of use case# 2: seasonal load restriction tool. In: FHWA-JPO-11-117.
C-SHRP, 2000. Seasonal load restrictions in Canada and around the world. In: Canadian Strategic Highway Research Program.
Fayer, M.J., Jones, T., 1990. UNSAT-H Version 2. 0: Unsaturated Soil Water and Heat Flow Model. Pacific Northwest Lab, Richland, WA (USA), Richiland, Washington.
Isotalo, J., 1993. Seasonal truck-load restrictions and road maintenance in countries with cold climate. In: Transport No. RD-14. Transportation, Water and Urban Development Department.
Jiji, L.M., Ganatos, P., 2009. Approximate analytical solution for one-dimensional tissue freezing around cylindrical cryoprobes. Int. J. Therm. Sci. 48 (3), 547–553.
Kestler, M.A., Knight, T., Krat, A., 2000. Thaw weakening on low volume roads and load restriction practices. In: US Army Cold Regions Research and Engineering Laboratory Technical Report TR00-6, Hanover, NH.
Konrad, J.-M., 1989. Physical processes during freeze-thaw cycles in clayey silts. Cold Reg. Sci. Technol. 16 (3), 291–303.
Lachance-Tremblay, É., Perraton, D., Vaillancourt, M., Di Benedetto, H., 2017. Degradation of asphalt mixtures with glass aggregates subjected to freeze-thaw cycles. Cold Reg. Sci. Technol. 141, 8–15.
Lai, Y., Liu, Y., Ma, D., 2014. Automatically melting snow on airport cement concrete pavement with carbon fiber grille. Cold Reg. Sci. Technol. 103, 57–62.
Liu, Z., Yu, X., 2014. Predicting the phase composition curve in frozen soils using index properties: a physico-empirical approach. Cold Reg. Sci. Technol. 108, 10–17.
Lu, J., Zhang, M., Zhang, X., Pei, W., Bi, J., 2018. Experimental study on the freezing–thawing deformation of a silty clay. Cold Reg. Sci. Technol. 151, 19–27.
Mahoney, J., Rutherford, M., Hicks, R., 1987. Guidelines for spring highway use restrictions. In: FHWA-TS-87-209. Federal Highway Administration.
Marquis, B., 2008a. Mechanistic Approach to Determine Spring Load Restrictions in Maine. Maine. Dept. of Transportation, Augusta, Maine.
Marquis, B., 2008b. Mechanistic Approach to Determine Spring Load Restrictions in Maine. Maine. Dept. of Transportation, Augusta, Maine.
McBane, J.A., Hanek, G., 1986. Determination of the Critical Thaw-Weakened Period in Asphalt Pavement Structures.
Miller, H., Cabral, C., Kestler, M., Berg, R., Eaton, R., 2012. Calibration of a freeze-thaw prediction model for spring load restriction timing in northern New England. In: Cold Regions Engineering 2012: Sustainable Infrastructure Development in a Changing Cold Environment. American Society of Civil Engineers, Quebec City, Canada, pp. 369–379.
Shoop, S., Affleck, R., Haehnel, R., Janoo, V., 2008. Mechanical behavior modeling of thaw-weakened soil. Cold Reg. Sci. Technol. 52 (2), 191–206.
Simonsen, E., Isacsson, U., 1999. Thaw weakening of pavement structures in cold regions. Cold Reg. Sci. Technol. 29 (2), 135–151.
Tighe, S.L., Mills, B., Haas, C.T., Baiz, S., 2007. Using Road Weather Information Systems (RWIS) to Control Load Restrictions on Gravel and Surface-Treated Highways. Ontario Ministry of Transportation, Downsview, Ontario Canada.
Van Deusen, D., Schrader, C., Bullock, D., Worel, B., 1998. Springtime thaw weakening and load restrictions in Minnesota. Transportation Research Record: Journal of the Transportation Research Board 1615, 21–28.
Xu, J., Ren, J., Wang, Z., Wang, S., Yuan, J., 2018. Strength behaviors and meso-structural characters of loess after freeze-thaw. Cold Reg. Sci. Technol. 148, 104–120.
Yin, X., Liu, E., Song, B., Zhang, D., 2018. Numerical analysis of coupled liquid water, vapor, stress and heat transport in unsaturated freezing soil. Cold Reg. Sci. Technol. 155, 20–28.
Zarrillo, M., Miller, H., Balasubramanian, R., Wang, H., Berg, R., Eaton, R., Kestler, M., 2012. Preliminary development of a real time seasonal load restriction system for remote sites. In: Cold Regions Engineering 2012: Sustainable Infrastructure Development in a Changing Cold Environment. ASCE, pp. 380–390.